

On the origin of atomistic mechanism of rapid diffusion in alkali halide nanoclusters

Tomoaki Niiyama,* Shin-ichi Sawada†, Kensuke S. Ikeda‡, and Yasushi Shimizu‡

College of Science and Engineering, Kanazawa University, Kakuma-machi, Kanazawa 920-1192, Japan

† Department of Physics, Kwansei Gakuin University, Gakuen 2-1, Sanda 669-1337, Japan

‡ Department of Physics, Ritsumeikan University, Noji-higashi 1-1-1, Kusatsu 525-8577, Japan

To elucidate the atomistic diffusion mechanism responsible for the rapid diffusion in alkali halide nano particles, called *Spontaneous Mixing*, we execute molecular dynamics simulations with empirical models for KCl-KBr, NaCl-NaBr, RbCl-RbBr and KBr-KI. We successfully reproduce essential features of the rapid diffusion phenomenon. It is numerically confirmed that the rate of the diffusion clearly depends on the size and temperature of the clusters, which is consistent with experiments. A quite conspicuous feature is that the surface melting and collective motions of ions are inhibited in alkali halide clusters. This result indicates that the *Surface Peeling Mechanism*, which is responsible for the spontaneous alloying of binary metals, does not play a dominant role for the spontaneous mixing in alkali halide nanoclusters. Detailed analysis of atomic motion inside the clusters reveals that the *Vacancy Mechanism* is the most important mechanism for the rapid diffusion in alkali halide clusters. This is also confirmed by evaluation of the vacancy formation energy: the formation energy notably decreases with the cluster size, which makes vacancy formation easier and diffusion more rapid in small alkali halide clusters.

I. INTRODUCTION

Over the past twenty years, a considerable amount of research of nano size materials, e.g., carbon nanotubes, quantum dots, nano particles, has been done owing to its technological importance [1, 2]. As is well known, nano particles play a key role for applications such as catalytic reactions in fuel cells [3, 4]. Though these nano size materials are widely manipulated and synthesized, it has been unclear how the materials are dynamically organized microscopically. In other words, fundamental dynamical aspects of nano materials such as transport mechanisms of atoms in small and finite materials have not been fully understood yet.

Meanwhile, the *rapid diffusion* which is a characteristic dynamical behavior peculiar to nano materials has been found experimentally in nano metal and alkali halide particles [5–9]. The experimental results reveal that the solid diffusion in nano clusters occurs considerably faster than the diffusion in bulk solids, and that such a rapid diffusion is enhanced by the smallness of the system. Elucidation of the atomistic process underlying this phenomenon lead us to a deeper understanding of the atomic motion in nano size material with a surface.

The rapid diffusion in metal nano particles, which is called *Spontaneous Alloying* (SA), has been experimentally observed *in situ*, for the first time, using transmission electron microscopy by Yasuda and Mori [5–7]. According to their observations, SA is the phenomenon that nano size core-shell type bimetallic clusters prepared by vacuum deposition of metal atoms onto a cluster of another kind of metal, e.g., gold clusters covered with copper atoms, quickly transform into homogeneous alloy clusters without melting even at room temperature. The time needed for the clusters to be alloyed is much shorter than that of bulk bimetals. A rough estimation tells that the diffusion of Au in nano clusters is nine orders of magnitude faster than that in bulk systems.

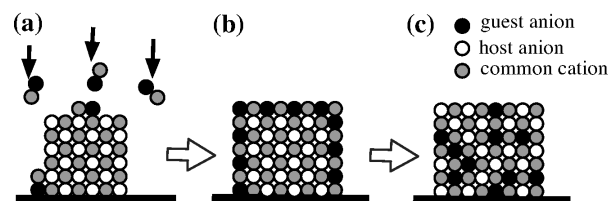


FIG. 1. Schematic illustrations for the process of Spontaneous Mixing. (a) After an AH nano cluster consists of host anion (white circles) and cations (grey circles) was prepared on a substrate, another kind of AH consist of guest anion (black circles) and common cations are deposited on the cluster by vacuum evaporation. (b) The AH cluster composed by host anions (white) and cations (grey) is gradually covered by another kind of AH having a common cation. (c) These ions of the cluster rapidly mix with each other at room temperature when the size of initial AH cluster is sufficiently small.

Shimizu and his coworkers have studied this very peculiar diffusion phenomenon by Molecular Dynamics (MD) simulations using two dimensional Morse models. They suggested that surface melting peculiar to nano metal clusters plays a crucial role in the onset of SA [10, 11]. It is well-known that the surface melting in a nano particle occurs even at a temperature considerably lower than its melting point. In their MDs, the surface melting was observed as frequent rearrangements of the surface atoms [12, 13]. They paid particular attention to the motion of core atoms which were initially encapsulated inside the cluster. They found that surface melting enables these core atoms to move collectively without breaking into pieces and thus expose themselves to the surface. The collection of core atoms is dispersed by the surface melting when it becomes part of the surface. The mixing process of the core atoms with the surface atoms caused by such an atomic motion is called as *Surface Peeling Mechanism* (SPM) [10, 11]. Moreover, it has been verified that the SPM similarly occurs in many-body potential models different from Morse type models. [14–16]. Restructuring of cluster shapes by complex collective motions has also been reported in growth simulations of binary metal clusters with many-body potential [17].

After Yasuda and Mori, a similar rapid diffusion has also

* ni-yama@ike-dyn.ritsumei.ac.jp

been observed experimentally in alkali halide (AH) nano clusters by Kimura and his coworkers, and they called it *Spontaneous Mixing (SM) phenomenon* [8, 9]. As shown by the schematic pictures of the phenomenon in figure 1, SM is rapid intermixing of AH clusters covered with another pair of alkali halide at room temperature. Kimura *et al.* found that SM occurs even in AH clusters as large as about 200 nano meter (nm) in size. This is much larger than the maximum size of metal clusters for which SA is observed. They pointed out the similarities between SA and SM, since they are both considered as a manifestation of rapid diffusion of constituent atoms peculiar to small clusters. However, there exists an essential difference between them. Kimura *et al.* concluded that one of the most important controlling factors of SM is the minimum ratio of ionic radii contained in AH clusters [8, 9]. However, at a microscopic level, the rapid diffusion mechanism of constituent atoms has not been clarified yet.

In this paper, we investigate the similarities and the essential differences between SM in AH clusters and SA in metal clusters at an atomistic level. In particular, we are much interested in whether the Surface Peeling Mechanism, which plays the key role in SA, is similarly important for SM, or not.

In section II, our numerical model together with our method of research are described, and the initial configurations and an indicator of intermixing, which are employed in the MD simulation, are introduced. In Sec. III, we show the results for the direct observation of the MDs, and quantitative analyses for the intermixing process, namely, the dependence upon temperature, cluster size, and the species of ions forming AH clusters are examined, paying particular care to checking whether the cluster is melting or not. We investigate the diffusion mechanism in Sec IV by observation of the motion of ions and vacancies inside the clusters, then show that ions in the clusters diffused by the Vacancy Mechanism. Finally, in Sec V, we discuss the rate of the diffusion observed in our MDs, and the reason for the rapidness of diffusion in small AH clusters.

II. MODEL AND NUMERICAL METHOD

A. Model

As stated in the introduction we investigate the SM by constant energy MD simulations. For this purpose, we consider the Hamiltonian which consists of N particles interacting with a two-body potential energy function $v(r_{ij})$

$$H = \sum_{i=1}^N \frac{\mathbf{p}_i^2}{2m_i} + \sum_{i<j}^N v(r_{ij}), \quad (1)$$

where r_{ij} is the distance between i -th and j -th ions, $|\mathbf{q}_i - \mathbf{q}_j|$, \mathbf{q}_i and \mathbf{p}_i are the configurational and momentum coordinate of i -th atom, m_i is the mass of i -th atom, respectively. For AH clusters, we employed the Coulomb plus Born-Mayer potential [18] given by

$$v(r_{ij}) = q_i q_j / r_{ij} + A_{k\ell} \exp \left[(R_k + R_\ell - r_{ij}) / \rho_{k\ell} \right], \quad (2)$$

where q_i indicates the charge of the i -th ion, k and ℓ denote species of the i -th and j -th ions, and $A_{k\ell}$, R_k and $\rho_{k\ell}$ are the Tosi-Fumi's parameters [19, 20], respectively. Since the original Tosi-Fumi model is applicable only for the single-species AH, we extend the Tosi-Fumi potential so as to be applicable to binary AH. That is, we used the arithmetic mean of two different anion's parameters $\rho_{k\ell}$ as the parameter between these different pair. For instance, $(\rho_{Cl-Cl} + \rho_{Br-Br})/2$ is used for ρ_{Cl-Br} , where ρ_{Cl-Cl} and ρ_{Br-Br} are the parameters for KCl and KBr, respectively. (Note that the value of the parameters, $\rho_{k\ell}$, for cation-cation and anion-anion interaction are assumed to be equal to the value of the parameter for cation-anion interaction in the Tosi-Fumi's model [19, 20].) In this paper, we denote an AH cluster consisting of alkali halides AB and CD as AB-CD, or $(AB)_n(CD)_m$ when n AB and m CD pairs constitute the cluster: for instance, NaCl-KBr or $(NaCl)_n(KBr)_m$.

For simplicity, we consider AH clusters which consist of only two different kind of anions and common cations e.g., KCl clusters covered with KBr ions. Now we name the anions inside the cluster like Cl as *host*, while we call the anions which are initially located at the surface like Br as *guest*. And we call such a cluster a *binary cluster*, because we are concerned with the intermixing between host and guest anions. In Fig. 1, cations, host anions and guest anions are shown by grey, white and black circles, respectively.

B. Initial configurations and numerical method

Next we explain the configurations of ions in a cluster at the initial time ($t = 0$). We employed the configurations in which several ions were removed from the cubic cluster with simple cubic lattice, specifically $(5 \times 5 \times 5 - 3)$, $(7 \times 7 \times 7 - 3)$ and $(9 \times 9 \times 9 - 3)$ structure (see Fig 2), where $(n \times n \times n - \alpha)$ denotes the resultant structure where α ions were removed from an edge of a cluster forming cubic structure composed of $n \times n \times n$ atoms. The reason for such a choice of initial configuration is that atomic vacancies and their migration are indispensable for intermixing in AH clusters to be initiated, as will be described later.

It is a difficult problem to prepare an "ideal" structure of the initial configuration for rapid diffusion, because the natural configurations of atoms in the initial stage has not been clarified in any experiments. If one chooses a *close-packed structure* as the initial configuration, [the $(n \times n \times n)$ cubic structure is one of the close-packed structures of AH nano particles which is quite stable], it is easily expected that no intermixing phenomenon will be observed. Due to the stability of the closed-packed structure one has to wait a very long time for any atom to migrate even to its nearest neighbor site. For this reason, we employed non-close-packed structures. (The stability and reliability of this type of non-close-packed structure has been discussed in experiments and ab initio calculations [21].)

To constitute an initial configuration, we firstly took a $[(n - 2) \times (n - 2) \times (n - 2)]$ cubic cluster which is constituted of host anions and cations. Next, we cover the cluster with a mono layer of alkali halides which consist of guest an-

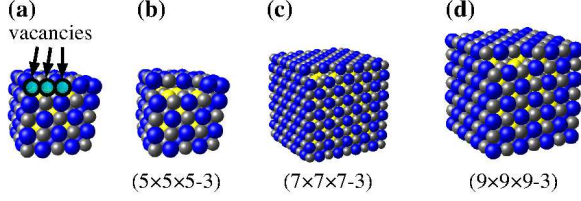


FIG. 2. Typical initial configurations for the MD simulations of AH clusters. Three ions were removed from one of the edges of $(n \times n \times n)$ shape AH clusters, i.e., there are three atomic vacancies on the edge, where guest, host anions and common cations are colored blue, yellow and grey.

ions and cations. Finally some ions (the total number is α) were removed from one of the twelve edges of the cubic cluster. We chose $\alpha = 3$ in this study. As a result, we prepared an initial configuration with three neighboring vacancies on a surface edge, as shown in Fig. 2.

We executed MDs under the isoenergetic condition by the velocity form of the Verlet algorithm, where the time step was typically 10 femto seconds. Numerical results described below are mainly based on the simulation of KCl-KBr clusters. We also mention some results of the simulation for NaCl-NaBr, RbCl-RbBr and KBr-KI clusters. Note that Cl and Br are respectively host and guest anions in KCl-KBr, NaCl-NaBr and RbCl-RbBr experiments, and that Br and I are respectively host and guest anions in KBr-KI experiments.

First of all, employing the velocity scaling method in time evolution we raised the temperature of a cluster having the initial configuration shown in Fig. 2 from ground state to a desired temperature. Here, we used the micro canonical kinetic temperature T defined by

$$T = \frac{2 \langle K \rangle}{(3N - 6)k_B}, \quad (3)$$

where $\langle K \rangle$, N and k_B are time-average of the total kinetic energy, the total number of the atoms and Boltzmann's constant, respectively [22, 23]. The factor 6 in the above equation results from the conservation of the total translational and angular momentum of the system under the isolated condition [24].

Then, after achieving the desired temperature, the cluster was evolved under the isoenergetic condition, where the total simulation time periods were from 200 to 2000 nano seconds (ns) depending on the situation. In each MD run, temperature T indicates an initial value of the micro canonical kinetic temperature. Since vibrational period is typically $10^{-1} - 10^0$ pico seconds (ps), we averaged every time series of the cluster configuration over a period of 10 ps, finally obtaining a series of configuration from which thermal vibration of the atoms was almost eliminated.

C. Indicator of mixing

In order to quantify the time evolution of the mixing process, let us introduce an indicator of intermixing. The intermixing requires motion of the guest atoms toward the center

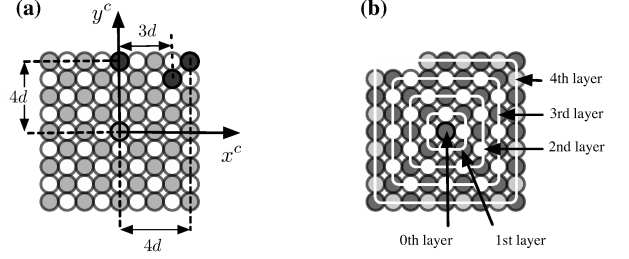


FIG. 3. A schematic figure of an AH cluster is represented by a two-dimensional square cluster. (a) A guest anion is colored by black, and host anions and common cations are represented by grey and white circles, respectively. In the case that the guest anion which is initially located at $(x^c, y^c) = (4d, 4d)$ occasionally hops along the surface to the lattice site $(x_c, y_c) = (0, 4d)$ (surface diffusion), the distance, r_i^c , keeps the constant value $4d$ during the hopping process. However, the distance, r_i^c , decreases to $3d$, when the initial guest anion hops to an inside site, e.g., $(x_c, y_c) = (3d, 3d)$. (b) We intentionally introduce atomic vacancies on the cluster surface by removing some atoms. The white lines indicate the layers which virtually decompose a cluster into parts. We define the index for the layers, which is allocated by ascending order from the surface, because it is helpful for a simple indication for the penetration depth of the guest anions (See SubSec. III D).

of a cluster, so we can use a measure of the average distance of the guest atoms from the center of the cluster as an indicator of mixing. If a cluster has spherical symmetry, the average distance of guest atoms from the center of a cluster, $r_g = \frac{1}{N_g} \sum_{i=1}^{N_g} r_i$, where $r_i = |\mathbf{q}_i - \mathbf{R}|$ and \mathbf{R} is the position of the center of the cluster, is suitable for an indicator of intermixing [10, 11, 14]. However, the present clusters have cubic symmetry. The value of r_g may vary even by a trivial movement of atoms along the surface such as surface diffusion, which can not be regarded as the intermixing. Therefore, we introduce another definition of distance that is the maximum of the distances from the center along the axes, defined by

$$r_i^c = |\mathbf{q}_i - \mathbf{R}| \equiv \max \{ |(\mathbf{q}_i - \mathbf{R}) \cdot \mathbf{e}_j|, j = 1, 2, 3 \}, \quad (4)$$

where \mathbf{e}_1 , \mathbf{e}_2 and \mathbf{e}_3 are the three independent vectors which are along the crystal axis and perpendicular to three surfaces of a cubic cluster. We shall call this the “principal radial distance”.

In Fig. 3 (b), a typical two dimensional example is shown. Each layer is denoted by 0th, 1st, \dots , ℓ -th, \dots , L -th layer from the center to the surface. The integer ℓ is the index of a layer. Note that 0th and L -th layer correspond to the center and surface of the cluster, respectively. When the i -th guest anion in a cubic cluster remains in the vicinity of its lattice point in the ℓ -th layer, the value of r_i^c is ℓd . Using the layer index, the average distance r_g is represented by $r_g = \frac{1}{N_g} \sum_{\ell=0}^L n_\ell \ell d$, where n_ℓ and N_g is the number of the guest anions in the ℓ -th layer and the number of all guest atoms, respectively. Note that the value r_g does not vary whenever any guest atoms move along a layer [see also Fig. 3 (a)]. Normalizing the average distance r_g by Ld , we here define the value R_g as an indicator of intermixing:

$$R_g(t) \equiv \frac{r_g}{Ld} = \frac{1}{N_g L} \sum_{\ell=0}^L n_\ell(t) \ell, \quad (5)$$

where $n_\ell(t)$ is the number of the guest atoms belonging to ℓ -th layer at time t .

In order to quantify the process of mixing, we estimate the ideal value for R_g that will be realized if the host and guest anions are homogeneously mixed. For this, let us assume a single AH cluster has $(N_g + N_h)$ lattice sites, where N_g and N_h are numbers of guest and host anions. We also assume that the guest anion occupies one of $(N_g + N_h)$ lattice sites with equal probability. Consequently the probability for finding a guest atom on an arbitrary lattice site for anions is $N_g/(N_g + N_h)$ when guest anions are spread homogeneously throughout a cluster by stochastic jumps. Thus, in such a mixed cluster the average number of the guest atoms in ℓ -th layer is represented by $\langle n_\ell \rangle = N_\ell N_g / (N_g + N_h)$, where N_ℓ is the number of the lattice sites for guests in ℓ -th layer. By substituting $\langle n_\ell \rangle$ to Eq. (5), one can derive the value R_g in an ideal mixed cluster,

$$\langle R_g \rangle = \frac{1}{(N_g + N_h)L} \sum_{\ell=0}^L N_\ell \ell. \quad (6)$$

For the $(5 \times 5 \times 5 - 3)$ cluster in Fig. 2, the number of the lattice sites for guests in each layer is $(N_0, N_1, N_2) = (0, 14, 47)$, and $L = 2$, $N_g = 47$, $N_h = 14$, so we obtain the ideal value $\langle R_g \rangle = 0.885$. Similarly, the ideal value is $\langle R_g \rangle = 0.852$ in a $(7 \times 7 \times 7 - 3)$ cluster, where $(N_0, N_1, N_2, N_3) = (0, 14, 48, 108)$, $L = 3$, $N_g = 108$ and $N_h = 62$. In a $(9 \times 9 \times 9 - 3)$ cluster, the ideal value is $\langle R_g \rangle = 0.829$, where $(N_0, N_1, N_2, N_3, N_4) = (0, 14, 48, 110, 189)$, $L = 4$, $N_g = 191$ and $N_h = 172$. By computing the value of the indicator R_g [Eq. (5)] with the value $\langle R_g \rangle$ for an ideal mixed cluster [Eq. (6)], one can quantify the degree of mixing during the SM.

III. DIRECT OBSERVATION AND QUALITATIVE ANALYSIS

A. Direct observation of intermixing in clusters

We show that AH clusters spontaneously mix without melting in the present MD simulations, where we employed KCl-KBr clusters: $(\text{KCl})_{14}(\text{KBr})_{47}$, $(\text{KCl})_{62}(\text{KBr})_{108}$ and $(\text{KCl})_{172}(\text{KBr})_{191}$ whose initial configurations are $(5 \times 5 \times 5 - 3)$, $(7 \times 7 \times 7 - 3)$ and $(9 \times 9 \times 9 - 3)$ structure as described in Subsec. II B, respectively. We chose the present AH cluster, because the SM for KCl-KBr clusters has been observed in the experiments [8, 9]. We executed isoenergetic MDs for $(\text{KCl})_{14}(\text{KBr})_{47}$ at 650 K ($E = -3.0985 \pm 0.0002$ eV/atom), $(\text{KCl})_{62}(\text{KBr})_{108}$ at 700 K ($E = -3.1441 \pm 0.0002$ eV/atom) and $(\text{KCl})_{172}(\text{KBr})_{191}$ at 800 K ($E = -3.1468 \pm 0.0002$ eV/atom), where E is the total energy of the system.

The snapshots taken at 10 ps intervals are shown in Fig. 4. As is evident from the figure, host anions (Cl^- , colored yellow) which have been located on the cluster's inside at $t = 0$ gradually aggregate on the surface by exchanging positions with guest anions (Br^- , colored blue) located on the surface at $t = 0$. During the entire time evolutions the clusters keep a

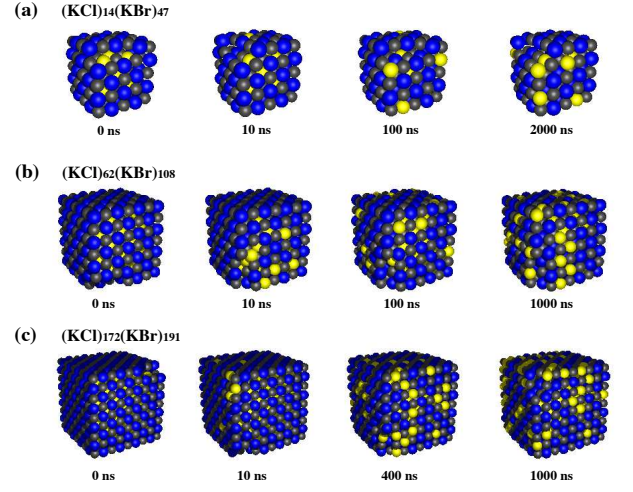


FIG. 4. Snapshots of the configuration of $(\text{KCl})_{14}(\text{KBr})_{47}$, $(\text{KCl})_{62}(\text{KBr})_{108}$ and $(\text{KCl})_{172}(\text{KBr})_{191}$ cluster in time evolution at 650, 700 and 800 K, respectively. The yellow-colored host anions (Cl^-), which were located inside the clusters at $t = 0$ gradually appeared on the surface in these clusters. This is a manifestation of the fact that host anions exchange positions with guest anions (Br^-) which are colored by blue.

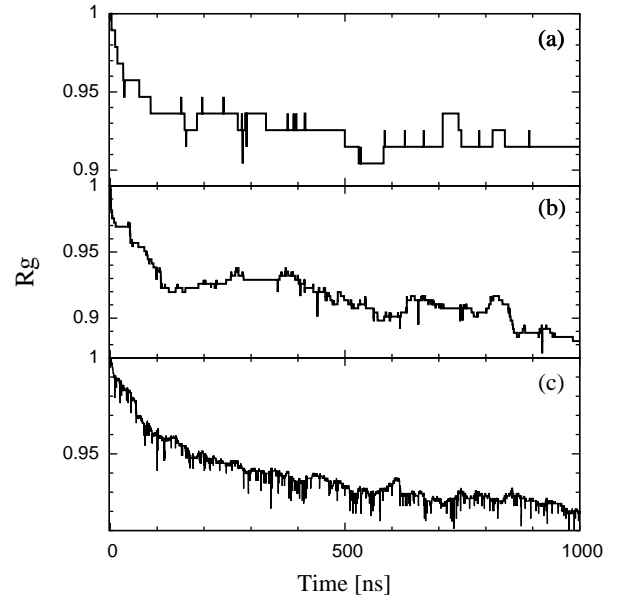


FIG. 5. Typical time evolutions of $R_g(t)$ for three different sizes of clusters. The initial temperature is higher for larger cluster size. (OR) The larger the cluster size, the higher the initial temperature. (a) $(\text{KCl})_{14}(\text{KBr})_{47}$ at 650 K. (b) $(\text{KCl})_{62}(\text{KBr})_{108}$ at 700 K. (c) $(\text{KCl})_{172}(\text{KBr})_{191}$ at 800 K.

simple cubic shape [25]. On the other hand, the three vacancies that are initially neighbors on a surface edge at $t = 0$ tend to move together on the edges of the cluster, with occasional independent excursions inside the cluster. (One can see the vacancies begin to move separately in Fig. 4 (b) at $t = 10$ ns).

Next we provide quantitative description of the progress of SM in the KCl-KBr clusters using the indicator R_g [Eq. (5)]. In Fig. 5 (a), we show typical time evolutions of $R_g(t)$ of $(\text{KCl})_{14}(\text{KBr})_{47}$ at $T = 650$ K, $(\text{KCl})_{62}(\text{KBr})_{108}$ at $T = 700$ K

and $(\text{KCl})_{172}(\text{KBr})_{191}$ at $T = 800$ K, corresponding to the case in Fig. 4. In Fig. 5 one can see that the value R_g is unity at $t = 0$. The initial value is $R_g(0) = 1$ by the definition. The value R_g decreases discontinuously with small spiky fluctuations as is seen in Fig. 5. This fluctuation can be smeared out by averaging with several samples of MD runs as shown in Fig. 8. The resultant averaged value shows a monotonous decreasing trend. However, the indicator $R_g(t)$ did not reach its ideal value $\langle R_g \rangle = 0.885$ over the time evolution. The behaviors of the other size clusters shown in Fig. 5 (b) and (c) are similar to those of $(\text{KCl})_{14}(\text{KBr})_{47}$ described in the above. That is, the way of intermixing is common to these three types of AH clusters at a qualitative level. It is evident that the intermixing tends to be suppressed in larger clusters. Because the intermixing is enhanced in smaller clusters, we hereafter call the present intermixing Spontaneous Mixing (SM).

Such intermixing in AH clusters is observed quite commonly in simulations where host anions are initially covered with guest anions. It is plausible to expect that these examples are manifestations of the SM which was experimentally observed.

B. Intermixing without melting

According to the experiments for SA, the completely intermixed state is attained without melting [5–7]. The completely intermixed state in AH clusters is also attained in a solid phase [8, 9]. It is necessary to confirm that the AH cluster in the present simulation is solid-like from beginning to end during SM. The snapshots in Fig. 4 show that the KCl-KBr clusters keep simple cubic shapes during the intermixing. Although it is obvious that the clusters did not melt by the direct observation of these snapshots, we give quantitative evidence of non-melting. The presence of melting is probed by the so-called Lindemann's index, which is a measure of the relative fluctuation of the distance between any two atoms as follows,

$$\delta = \frac{2}{N(N-1)} \sum_{i < j}^N \frac{\sqrt{\langle r_{ij}^2 \rangle - \langle r_{ij} \rangle^2}}{\langle r_{ij} \rangle}, \quad (7)$$

where N is the number of atoms in the system, and $\langle r_{ij} \rangle$ is the long-time average distance between i -th and j -th atom [26]. When δ is larger than 0.1, the system is empirically considered to be melted. We verify that an averaging interval of 100 ps is long enough for the value of the index to be well averaged.

In Fig. 6, we show the typical time evolution of δ during SM for $(\text{KCl})_{14}(\text{KBr})_{47}$, $(\text{KCl})_{62}(\text{KBr})_{108}$ and $(\text{KCl})_{172}(\text{KBr})_{191}$, corresponding to Fig. 4 and Fig. 5. The values of δ for $(\text{KCl})_{14}(\text{KBr})_{47}$, $(\text{KCl})_{62}(\text{KBr})_{108}$ and $(\text{KCl})_{172}(\text{KBr})_{191}$ are about 0.05, 0.04 and 0.03, respectively. These are sufficiently smaller than the melting criterion 0.1, thus the SM for KCl-KBr clusters is considered to proceed in solid phase.

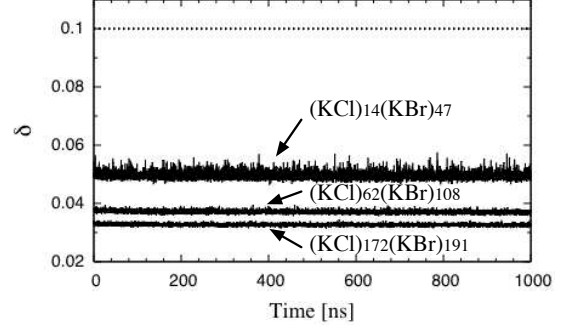


FIG. 6. Typical time evolution of Lindemann's index δ during SM for $(\text{KCl})_{14}(\text{KBr})_{47}$, $(\text{KCl})_{62}(\text{KBr})_{108}$ and $(\text{KCl})_{172}(\text{KBr})_{191}$.

C. Dependence upon ion species

To see the dependence of SM upon the choice of ion species, we examined several combinations of alkali halides such as NaCl-NaBr, RbCl-RbBr and KBr-KI, in addition to KCl-KBr. For comparison, $(\text{NaCl})_{14}(\text{NaBr})_{47}$, $(\text{RbCl})_{14}(\text{RbBr})_{47}$ and $(\text{KBr})_{14}(\text{KI})_{47}$ with initial structure $(5 \times 5 \times 5 - 3)$ were employed, and the MD simulations for each cluster were done by setting the initial temperatures as $T = 600$ K.

The time evolution of $R_g(t)$ obtained by averaging over 5 MD runs is depicted in Fig. 7 (a). The figure shows that all the values of the averaged distance R_g s decrease monotonically and their behaviors are similar to that of KCl-KBr ones. In fact, one can verify that R_g for $(\text{KCl})_{14}(\text{KBr})_{47}$, $(\text{NaCl})_{14}(\text{NaBr})_{47}$ and $(\text{KBr})_{14}(\text{KI})_{47}$ exhibits a common decreasing rate, while $(\text{RbCl})_{14}(\text{RbBr})_{47}$ shows a rather slow decreasing trend. Note that R_g does not reach the ideal value, $\langle R_g \rangle = 0.885$, in all cases.

Typical time evolutions of Lindemann's index, δ , are depicted in Fig. 7 (b), where the points are plotted with 200 ps interval. During SM, all the values of δ are about 0.05 which is smaller than the melting criterion 0.1. Therefore, these clusters similarly show full intermixing in solid phase without exception.

According to the experiment for AH clusters by Kimura *et al.*, one of the dominantly controlling factors of SM is the minimum ratio of ionic radii of alkali halide constituent of clusters. More precisely, the intermixing occurred in the clusters whose minimum ratio of the ionic radii is larger than 68 % [8, 9]. According to this criterion, KCl-KBr and RbCl-RbBr clusters should exhibit intermixing, because the ratios of radii between cation and anion are $(\text{K}/\text{Br} = 0.68)$, $(\text{Rb}/\text{Br} = 0.76)$ and $(\text{K}/\text{Cl} = 0.73)$, respectively. On the contrary, one should expect the absence of intermixing in NaCl-NaBr and KBr-KI clusters $(\text{Na}/\text{Br} = 0.5)$ and $(\text{K}/\text{I} = 0.62)$, where the ratio of the radii of anions, Cl/Br and Br/I are 0.93 and 0.90, respectively. However, the present simulation results predict that there exists intermixing in NaCl-NaBr cluster like in other AH clusters. This discrepancy suggests that the dependence will be

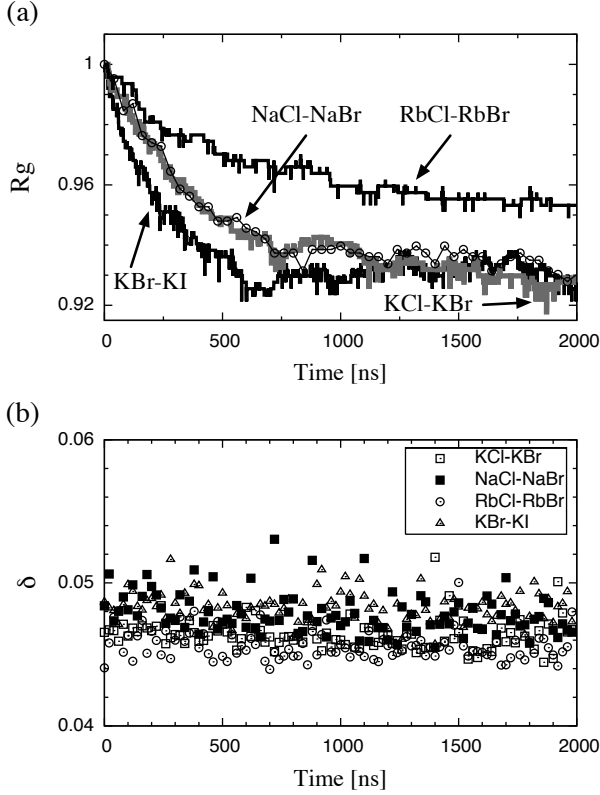


FIG. 7. Typical time evolution of (a) R_g and (b) Lindemann's indices δ for $(\text{KCl})_{14}(\text{KBr})_{47}$, $(\text{NaCl})_{14}(\text{NaBr})_{47}$, $(\text{RbCl})_{14}(\text{RbBr})_{47}$ and $(\text{KBr})_{14}(\text{KI})_{47}$ at $T = 600$ K.

reversed in smaller AH clusters such as in our MD's results, because the clusters employed in the experiments are much larger than those used in our simulations (the size of clusters in the experiments was several hundred nano meters).

D. Temperature-dependence

According to Yasuda and Mori, SA is enhanced for metal clusters, as the temperature is raised. However, no experimental observation showing the role of temperature is known for SM in AH clusters. In this subsection, we probe the temperature-dependence of intermixing in AH clusters. We calculated the time for $R_g(t)$ to reach a certain value for various initial temperatures.

The MD trajectories for $(\text{KCl})_{14}(\text{KBr})_{47}$ at the initial temperatures, $T = 500, 550, 600, 650$ and 700 K, were computed for five different initial conditions, respectively. The behaviors of $R_g(t)$ averaged over 5 samples for each temperature are shown in Fig. 8 (a). The results for $(\text{KCl})_{62}(\text{KBr})_{108}$ ($T = 600, 650, 700, 750, 800$ K) and $(\text{KCl})_{172}(\text{KBr})_{191}$ ($T = 650, 700, 750, 800, 850, 900$ K) are also depicted in Figs. 8 (b) and (c), respectively. The figures clearly demonstrate that $R_g(t)$ of all the clusters tend to decrease faster as the temperature is raised. In short, raising temperature promotes the diffusion in binary AH clusters. This dependence on temperature is quantitatively

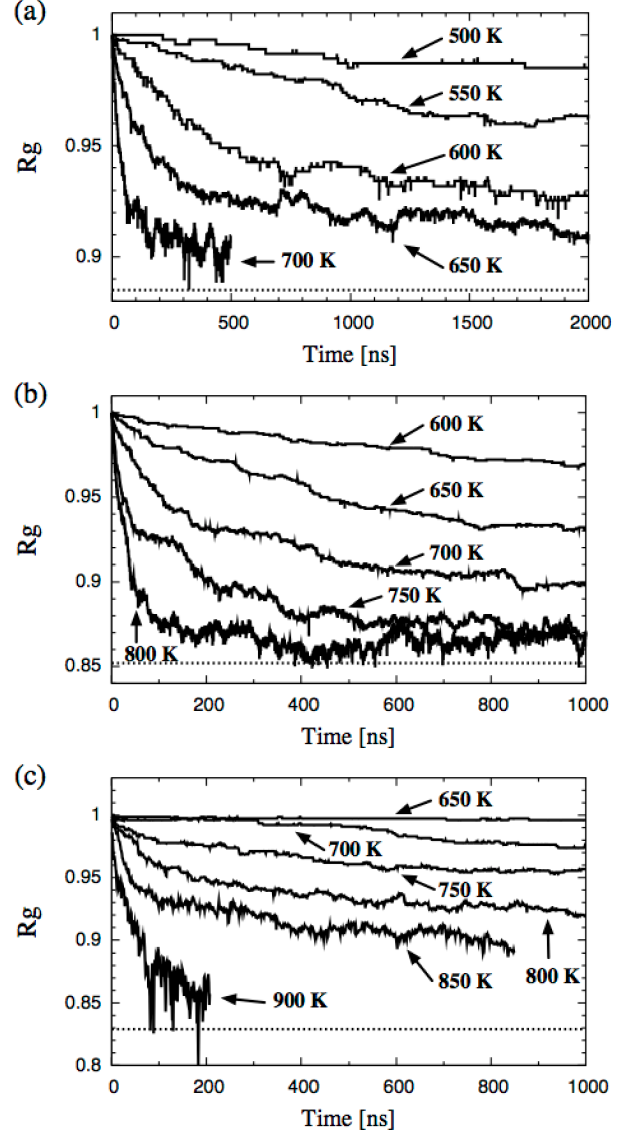


FIG. 8. Time evolution of the averaged distance $R_g(t)$ depending on various initial temperatures. The dot lines represent the ideal averaged distance $\langle R_g \rangle$ corresponding to a realization of perfect intermixing between host and guest anions. Three kinds of AH clusters are shown in (a) $(\text{KCl})_{14}(\text{KBr})_{47}$. (b) $(\text{KCl})_{62}(\text{KBr})_{108}$. (c) $(\text{KCl})_{172}(\text{KBr})_{191}$, respectively.

consistent with the conventional diffusion process and other studies of metal nano particles [10, 11, 14–16]. Arrhenius law for a diffusion of atoms in solid yields a well-known formula for the diffusion rate D as a function of temperature T :

$$D = D_0 \exp(-E_{act}/k_B T), \quad (8)$$

where D_0 , and E_{act} are a frequency factor and the activation energy of the diffusion, respectively [27, 28].

It is difficult to evaluate a diffusion rate of guest anions in clusters, because a large portion of surface atoms leads to the spatial-dependence of the diffusion rate. Instead of evaluating the diffusion rate, we focus our attention to the time τ required

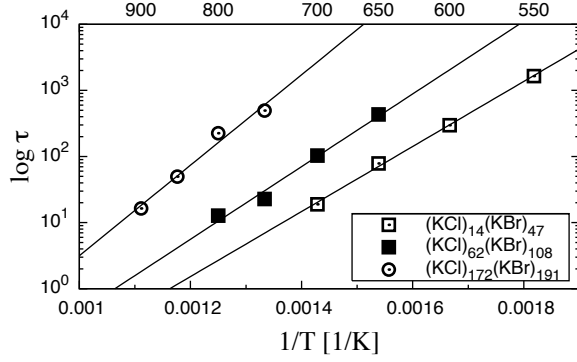


FIG. 9. The temperature dependence of the mixing time τ of $(\text{KCl})_{14}(\text{KBr})_{47}$, $(\text{KCl})_{62}(\text{KBr})_{108}$ and $(\text{KCl})_{172}(\text{KBr})_{191}$. The three solid lines, which represent Arrhenius type temperature dependence, are fitted by the least-squares method [Eq. (10)].

for R_g to reach a specific value R'_g ,

$$R_g(\tau) = R'_g. \quad (9)$$

We consider τ as the mixing time, and examine its temperature-dependence. Due to the difficulty of the choice R'_g , we tentatively employed the criteria $R'_g = \langle R_g \rangle + 2/3(R_g(0) - \langle R_g \rangle)$; the criteria of $(\text{KCl})_{14}(\text{KBr})_{47}$, $(\text{KCl})_{62}(\text{KBr})_{108}$ and $(\text{KCl})_{172}(\text{KBr})_{191}$ are $R'_g = 0.962$, 0.951 and 0.943 , respectively.

The semi-log plot of the inverse temperature versus the mixing time τ is depicted in Fig. 9. The three lines in the figure are obtained by assuming Arrhenius type temperature-dependence,

$$\tau = \tau_0 \exp(E_{act}/k_B T). \quad (10)$$

Two parameters, E_{act} and the frequency factor τ_0 are decided by the least-squares method. For $(\text{KCl})_{14}(\text{KBr})_{47}$, $(\text{KCl})_{62}(\text{KBr})_{108}$ and $(\text{KCl})_{172}(\text{KBr})_{191}$, we obtained $E_{act} = 0.98$, 1.1 and 1.4 eV and $\tau_0 = 1.9 \times 10^{-6}$, 1.4×10^{-6} , 4.6×10^{-7} ns, respectively.

One can see that the behavior of τ for the KCl-KBr clusters in Fig. 9 well follows the Arrhenius type law by choosing suitable values for the fitting parameters. The present result is consistent with the previous MD studies for SA [10, 11, 14–16]. That is, the time to accomplish the SM becomes longer in an exponential way, as the temperature is decreased, as in the case of SA.

E. Size-dependence

As is shown in the previous section, SA and SM have similarities in their time-dependent features. One may thus expect that other features of SM are also similar to those of SA. However, systematic studies for SM in AH cluster have been left untouched, whereas extensive experimental and theoretical studies have been done for SA. For instance, the size-dependent feature of SM has not been fully understood yet,

while it is well-known that SA is suppressed for the larger metal nanoclusters. In spite of the lack of systematic experimental studies for SM, it is reasonable to expect that SM will be suppressed for larger AH clusters.

To confirm such an expectation, we examine the size-dependent property of intermixing in KCl-KBr clusters. In particular, we put our emphasis upon the time, τ_g , required for guest atoms to migrate over a certain fixed distance, say Δr_g , and examine the size-dependence of τ_g . Here we employed $0.076d$ Å as the value of Δr_g , then evaluated τ_g for this value from data in Fig. 8.

To do that, we have to remark on the relation between Δr_g and R_g because Fig. 8 shows only the time evolutions of R_g , not Δr_g . Using average distance r_g between guest atoms and the center of a cluster, Δr_g is expressed as $\Delta r_g = r_g(0) - r_g^*$, where $r_g(0)$ is the distance at the initial time and r_g^* is that at the given time. Note that $r_g(0)$ and r_g^* depend on the cluster size. As mentioned in Subsec. IIC, the averaged distance is represented by $r_g(t) = LdR_g(t)$, where d is the lattice constant in a simple cubic structure. Thus, the migration length of the guest anions is alternatively expressed in terms of the normalized distance $R_g(t)$ as

$$\Delta r_g = Ld(R_g(0) - R_g^*) = Ld(1 - R_g^*). \quad (11)$$

Let us recall that $(\text{KCl})_{14}(\text{KBr})_{47}$, $(\text{KCl})_{62}(\text{KBr})_{108}$ and $(\text{KCl})_{172}(\text{KBr})_{191}$ clusters form $(5 \times 5 \times 5 - 3)$, $(7 \times 7 \times 7 - 3)$ and $(9 \times 9 \times 9 - 3)$ structures, and the number of their layers is $L = 2$, 3 and 4 , so the corresponding values of R_g^* for $\Delta r_g = 0.076d$ Å are $R_g^* = 0.962$, 0.975 and 0.981 , respectively. Therefore, τ_g can be translated as the time when $R_g(t)$ reaches 0.962 , 0.975 and 0.981 for $(\text{KCl})_{14}(\text{KBr})_{47}$, $(\text{KCl})_{62}(\text{KBr})_{108}$ and $(\text{KCl})_{172}(\text{KBr})_{191}$, respectively.

For evaluating τ_g , we chose the MD results at 700 K shown in Fig. 8. With these data we obtained $\tau_g = 18.9$, 42.1 , and 668 ns for $(\text{KCl})_{14}(\text{KBr})_{47}$, $(\text{KCl})_{62}(\text{KBr})_{108}$ and $(\text{KCl})_{172}(\text{KBr})_{191}$ clusters, respectively. Thus, the time required by guest anions to diffuse over the distance increases very rapidly with an increase in the size of the cluster, which means that the SM is inhibited in larger clusters. In this sense, we verified the similarities in the size-dependence between SM and SA.

Furthermore, it is worth to emphasize that we also confirm the same aspect of the size-dependence in Fig. 9. As mentioned in the previous subsection, the activation energy introduced in Eq. (10) becomes larger for the larger AH cluster. In both cases, we ascertain that the size of AH cluster affects the mobility of guest anions entering the center of the cluster.

IV. DIFFUSION MECHANISM

We showed that intermixing in AH clusters occurred spontaneously in solid phase. In this section, we explore some details of the atomistic diffusion mechanism of the intermixing. Firstly, we attempt to quantify the onset of surface melting which is considered to be a necessary condition for the Surface Peeling Mechanism. Then we characterize the motion

of atoms inside a cluster by focusing attention on the core of the cluster. The results of these observations imply that the diffusion mechanism of intermixing is the so-called Vacancy Mechanism [27]. Finally, by visualizing trajectories of all ions of an AH cluster we present direct evidence indicating that the diffusion is governed by the Vacancy Mechanism.

A. Surface melting

Surface melting of metal clusters which occurs even at temperatures considerably lower than their melting points has been reported in some experimental studies [12, 13, 29]. As mentioned in Sec. I, the surface melting is one of the necessary conditions for the Surface Peeling Mechanism to work. Indeed, the previous results based on 2D Morse model show how surface melting enhances SA by the Surface Peeling Mechanism [10, 11]. Therefore, it is plausible to expect that the same mechanism similarly works in SM of AH clusters. In this subsection, we verify the absence of surface melting on AH clusters during SM.

Following the previous study [11], we defined the Lindemann's index for the i -th atom,

$$\delta_i = \frac{1}{N-1} \sum_{j \neq i}^N \frac{\sqrt{\langle r_{ij}^2 \rangle - \langle r_{ij} \rangle^2}}{\langle r_{ij} \rangle}, \quad (12)$$

and called it *the individual Lindemann's index*. This index is an extension of the Lindemann's index introduced in Subsec. III B. The quantitative signature of surface melting is that the indices of surface atoms are significantly larger than those of inner atoms.

Here, we show the MD result of SM in $(\text{KCl})_{172}(\text{KBr})_{191}$ as an example. The mean square displacement between i -th and j -th ions, $\langle r_{ij}^2 \rangle - \langle r_{ij} \rangle^2$, which is averaged over a 10 ps interval is computed. At the same time the principal radial distance of i -th ion r_i^c was also recorded. Then one thousand samples of i -th ion's Lindemann index δ_i were obtained as a function of r_i^c . In Fig. 10, we show δ_i as a function of r_i^c at $T = 600, 700, 800$ and 900 K averaged over the interval of 0.5 Å.

It is evident that δ_i is $0.02 - 0.04$ and almost constant over the entire cluster except the range $r_i^c > 16$ Å. Increasing of δ_i in this range is so abrupt that one might consider the surface is in a melting state. However, it is not true due to the following reason: almost all the surface ions of $(\text{KCl})_{172}(\text{KBr})_{191}$ are at about $r_i^c = 14$ Å so that there are no ions at the range $r_i^c > 16$ Å. One of the insert figures in Fig. 10 is the snapshot of the time evolution of $T = 900$ K at 3.48 ns. At this moment, only five ions (two K^+ and three Br^-) were present on a surface of the cluster: ions whose positions r_i^c are $19.3, 18.1, 16.8, 16.6$ and 20.8 Å and indices δ_i are $0.0782, 0.0538, 0.0391, 0.0729$ and 0.0736 , respectively. On the other hand, the other ions remain on their lattice sites. Thus, the abrupt increasing of δ_i at the range $r_i^c > 16$ Å is due to such a type of rare events. One can also confirm this from the other insert figure in Fig. 10 representing the distribution of ions as a function of r_i^c . The figure clearly shows that the relative

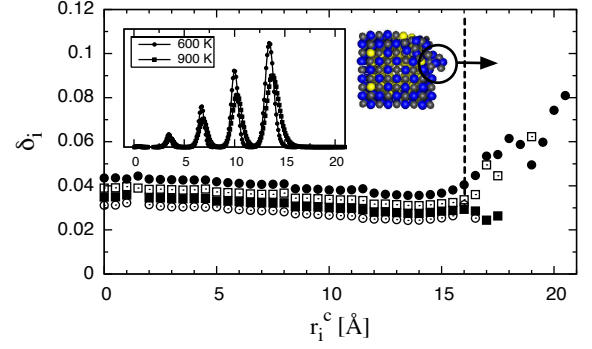


FIG. 10. Individual Lindemann's index δ_i in $(\text{KCl})_{172}(\text{KBr})_{191}$ as a function of principal radial distance r_i^c (white circles, solid squares, white squares and solid circles are the values at 600, 700, 800 and 900 K, respectively). The frequency distribution of ions at 600 and 900 K is imposed as a function of r_i^c .

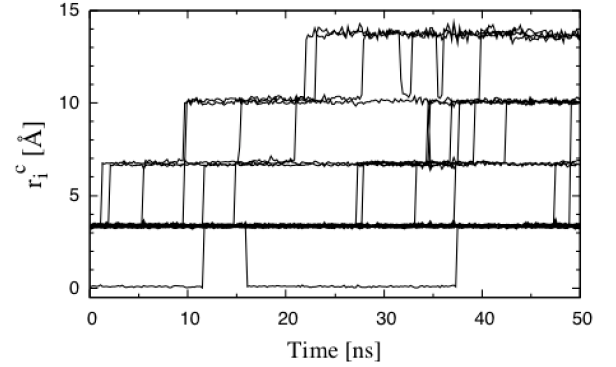


FIG. 11. Typical time evolutions of radial distance of individual ions r_i^c in $(\text{KCl})_{172}(\text{KBr})_{191}$ corresponding to the run as depicted in Fig. 4 (c).

frequency of ions appearing at the range $r_i^c > 16$ Å is significantly small. Therefore, the large value of δ_i , which is attributed to exceptional atomic motion, has to be ignored when judging the presence of the surface melting.

Thus, the numerical results concerning the individual Lindemann's index clearly show that the surface of $(\text{KCl})_{172}(\text{KBr})_{191}$ is not in a melting state during SM. The absence of surface melting in alkali halide systems is consistent with the result by Zykova-Timan *et al.* [30]. It strongly suggests that the Surface Peeling Mechanism does not contribute to the intermixing of AH clusters, unlike metal clusters.

B. Characteristic motion of core ions

In this subsection, we illustrate the characteristic motion of core ions in $(\text{KCl})_{172}(\text{KBr})_{191}$ during intermixing by observing the radial distance and by visualizing the projected positions of the ions. We will come to the following fact: Both results demonstrate that diffusion of the ions is dominated by the Vacancy Mechanism.

Let us summarize how the diffusion mechanism manifests

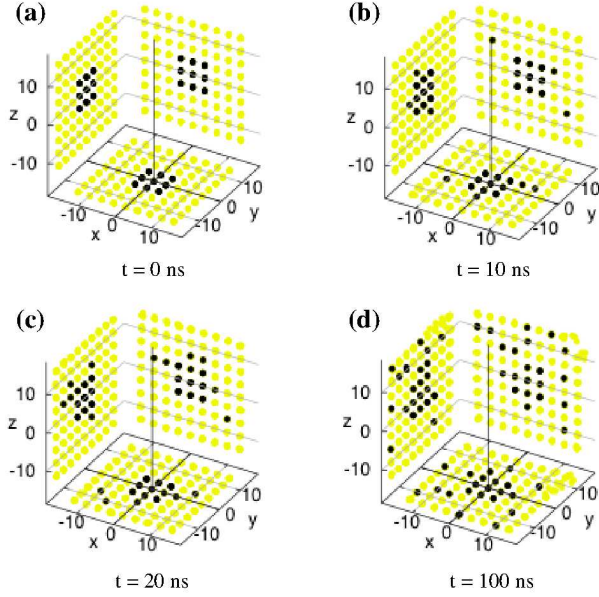


FIG. 12. The snapshots of the ions of $(\text{KCl})_{172}(\text{KBr})_{191}$ projected to x - y , y - z and z - x planes. The time evolution corresponds to cases shown in Figs. 4 (c) and 11. The black and yellow solid circles are the ions on $3 \times 3 \times 3$ central cubic lattice sites at $t = 0$ and the other ions, respectively.

in a characteristic motion of ions. If either vacancy or interstitial mechanism is responsible for the intermixing of AH clusters, then core ions of the cluster have to diffuse individually and separately. In contrast, the core ions tend to move simultaneously in case that the Surface Peeling Mechanism is responsible for SM, because the cluster core is solid-like in the present simulation. Thus, we can identify the diffusion mechanism that governs the SM by focusing on the motion of core ions in AH cluster.

Next, we pick up the 27 core ions which are initially located on $(3 \times 3 \times 3)$ lattice sites at the center of the cluster. The initial configuration of 27 core atoms is shown in Fig. 12 (a). The radial distance between the 27 core ions and the center, say r_i^c , is computed during SM. Notice that r_i^c was previously introduced in Subsec. III A. The time evolution of r_i^c for $(\text{KCl})_{172}(\text{KBr})_{191}$ is depicted in Fig. 11.

It is obvious that the plots corresponding to $r_i^c = 0 \text{ \AA}$ at $t = 0$ keeps on the horizontal line during $t = 0 - 11$ and $17 - 36$ ns. This means that the center ion yielding $r_i^c = 0 \text{ \AA}$ keeps its position during these two periods. In contrast, the plots corresponding to $r_i^c = 2.8 \text{ \AA}$ at $t = 0$ tend to jump among the various horizontal lines. That indicates that 26 ions which are initially belonging to core ions often move around from site to site. In other words, a single ion at the center stays at the same site for a long time, while the surrounding 26 atoms often hop from one layer to another individually and separately. The present behavior of the core 27 ions and the absence of surface melting are incompatible with the description of Surface Peeling Mechanism. Consequently, it strongly suggests that the diffusion inducing SM is caused by the Vacancy Mechanism.

We evaluate $r_i^c = 0 \text{ \AA}$ in the above, because in 3D model,

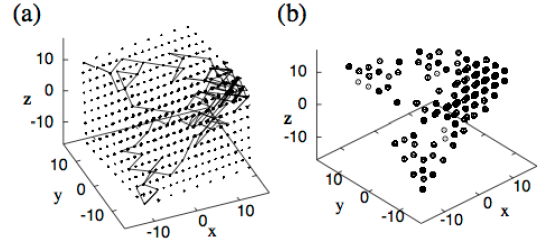


FIG. 13. (a) Trajectories of all ions of $(\text{KCl})_{172}(\text{KBr})_{191}$ are plotted during $t = 38.1 - 39.4$ ns. The line trajectories are due to hopping of ions. (b) All lattice sites occupied by a vacancy during $t = 38.1 - 39.4$ ns are displayed by circles.

it is difficult to visualize the motion of the hidden core atoms directly in 3D space. Here we visualize the diffusion process of interior ions of AH clusters by extracting the projected positions of ions onto three planes. More specifically, we look into the projected coordinates of all atoms on x - y , y - z and z - x planes.

In Fig. 12, we show snapshots of the projected positions of all the ions which are obtained from MD data for $(\text{KCl})_{172}(\text{KBr})_{191}$ during $t = 0 - 100$ ns. This corresponds to the time evolution shown in Figs. 4 (c) and 11.

The position of the core ions are prepared to form simple $(3 \times 3 \times 3)$ cubic structure. These core ions are initially located in the vicinity of the center of the cluster. These initial core ions are depicted by black circles, whilst the other 699 ions surrounding 27 core ions are colored yellow.

The results show that several core ions (black solid circles) diffuse and reach the cluster surface. But most initial core ions remain at the center. Moreover, there are no correlated motions of core ions in the snapshots. These snapshots also support the previous observation indicating that the Vacancy Mechanism is responsible for accomplishing SM in AH clusters. Thus, SM seems to originate from the combined effect of the individual diffusion of ions realized by the Vacancy Mechanism.

C. Visualization of the vacancy motion

A straightforward way to illustrate the crucial role of the Vacancy Mechanism is to visualize the motion of a vacancy itself. To do this, we put our focus on the events causing sudden changes of $\langle r_i \rangle$ in Fig. 11 which presents a visualization of atomic motion. The trajectories of all the ions in $(\text{KCl})_{172}(\text{KBr})_{191}$ are shown in Fig. 13 (a) during the period of $t = 38.1 - 39.4$ ns. A large number of dots and line segments form three zigzag lines. One longer entangled line forms a single loop, and the other two relatively short lines are overlapped with the longer line (the two shorter lines cannot be distinguished from the longer line). The dots mean that ions stay for a long time on their lattice points. The broken lines indicates the single hop of an ion from one occupied site to its second-neighbor unoccupied site, which is nothing more than the so-called vacancy site. Conversely, one can say that each of the broken lines indicates a hopping of a vacancy in a di-

rection opposite to the ion. One can conclude from Fig. 13 (a) that some ions hop from one site to another site so as to fill the vacancy created by a prior jump of another ion. On the other hand, almost all ions remain on the same lattice sites. One can reconfirm this picture by comparing Figs 13 (a) and (b). The circles in the latter figure indicate the lattice points occupied by a vacancy in a particular period $t = 38.1 - 39.4$ ns. The atomic trajectories depicted by the zigzag lines in the former figure correspond to the vacancy sites depicted by circles in the latter figure. This figure makes manifest that the atomic trajectory is equivalent to the vacancy trajectory.

It is hard to see the detail, but there coexist three zigzag lines in Fig. 13, corresponding to the trajectories of three vacancies in the cluster. The starting points of the vacancies are located on the edge of the initial configuration having a simple cubic structure. As shown in Fig. 2, these three vacancies are initially aligned along an edge. In Fig. 13, this vacancy trajectory forms a round trip loop — it starts from one of the surface vacancy sites, wanders deep inside the cluster, and eventually reaches the surface again.

It takes a relatively short period of time for a vacancy to travel along the loop. During the simulation time over 50 ns, there appear many loops corresponding to the frequent motion of vacancies everywhere inside of $(\text{KCl})_{172}(\text{KBr})_{191}$. The formation of vacancy hopping paths inside the cluster, is quite important to realize intermixing in $(\text{KCl})_{172}(\text{KBr})_{191}$. In this way, we are convinced that the SM is dominated by the *Vacancy Mechanism*.

V. DISCUSSIONS

The above numerical results gave evidence that binary AH clusters can spontaneously intermix even below their melting points. At a microscopic level, this intermixing is governed by migration of vacancies. The vacancies mediated diffusion is by no means a process specific to nanoclusters, but an ordinary process observed also in bulk AH crystal. Although the transport process is the same, why is the mixing process in an AH cluster much faster than in bulk AH? By analyzing the dominant factor controlling the diffusion rate in an AH cluster, we discuss the reason why the vacancy mechanism induces unexpectedly rapid diffusion in AH clusters.

A. Diffusion rate in AH clusters

Firstly, to demonstrate how rapid SM is, we roughly evaluate the diffusion rate in AH clusters by using MD data [6, 7]. Comparing the diffusion rate in cluster to that in bulk crystal shows how fast the SM is. By comparing the diffusion rate in cluster to that in bulk crystal, one might realize how fast the SM is. In general, it is difficult to estimate the diffusion rate in finite systems, where the surface diffusion coexists with bulk diffusion. Neglecting the spatial inhomogeneity due to the presence of the boundary, let us assume that diffusion rate is the same everywhere in the cluster. This simplification enables us to estimate the diffusion rate by τ , which

is the time spent by the guest atoms migrating over a distance, say $\Delta r'_g$. Note, however, that such a crude estimation often leads to an underestimation. The times required to diffuse over a distance $\Delta r'_g = 0.076d \text{ \AA} = 0.024 \text{ nm}$ at 700 K in $(\text{KCl})_{14}(\text{KBr})_{47}$, $(\text{KCl})_{62}(\text{KBr})_{108}$ and $(\text{KCl})_{172}(\text{KBr})_{191}$ are evaluated as $\tau = 18.9, 42.1$ and 668 ns, according to the data in Fig. 8. The resultant diffusion rates of the clusters are $D = 3.1 \times 10^{-14}, 1.4 \times 10^{-14}$ and $8.6 \times 10^{-16} \text{ m}^2/\text{s}$, respectively.

Secondly, we estimate the rate of lattice diffusion in bulk AH crystal for comparison. The diffusion rate by the Vacancy Mechanism in solids is usually represented by

$$D = D_0 \exp \left[-(E_f + E_m)/k_B T \right], \quad (13)$$

where D_0 is a constant factor, and E_f and E_m are the vacancy formation and migration energy, respectively. The sum of E_f and E_m is the activation energy of vacancy diffusion E_{act} . For instance, the energies in bulk KCl and NaCl crystals are approximately $E_f^S \approx 2 \text{ eV}$ and $E_m \approx 0.9 \text{ eV}$, respectively [28]. Since E_f^S is Schottky vacancy formation energy for an anion-cation pair, the formation energy of a single vacancy on an anion site is roughly estimated to be a half of E_f^S , i.e., $E_f \approx 1 \text{ eV}$. For *binary* AH crystals containing two different types of anions such as KCl-KBr, only a limited number of experimental studies have been done to exploring the atomic diffusion. In particular, based on experimental results, Pehkonen and his coworkers estimated the activation energy in KCl-KBr powder mixtures as $E_{act} = 2.1 \pm 0.1 \text{ eV}$ [31, 32]. According to their results, the activation energy of bulk AH crystals is approximately 2 eV. The constant factor is also roughly estimated as $D_0 = 1 \times 10^{-4} \text{ m}^2/\text{sec}$ by experiments [33, 34]. Then, by substituting these values into Eq. (13) we obtain the diffusion rate in bulk KCl-KBr crystals at 700 K; $D_{bulk} \approx 4.0 \times 10^{-19} \text{ m}^2/\text{s}$. In addition, we also obtain the diffusion time τ as follows; $\tau = 1.5 \times 10^6 \text{ ns}$ for $\Delta r'_g = 0.076d \text{ \AA}$.

The value τ in the clusters $\tau = 18.9\text{--}668 \text{ ns}$ is at least about four orders of magnitude less than τ in bulk solids. The diffusion rate D in the clusters is, at least, about two orders of magnitude larger than the one in bulk. The activation energy of the diffusion 0.98 - 1.4 eV estimated in Sec. IIID is significantly lower than that of the bulk diffusion. Taking into account these results, it is reasonable to conclude that the SM in the MD simulations is a significantly more rapid diffusion.

B. Principal origin of enhanced intermixing

Up to now, the reason why the diffusion rate in AH cluster is significantly more rapid than in AH bulk has not been clarified. At first sight, there seems to be no qualitative difference between the diffusion in bulk and that in a cluster. In this subsection, we discuss the factor enhancing the diffusion in AH clusters from the viewpoint of the size-dependence of *vacancy formation energy* E_f . In particular, we will demonstrate a decreasing trend of the formation energy with reducing size of AH cluster. This provides evidence that reduction of the

cluster size makes it energetically easier to generate vacancies causing SM.

The diffusion rate controlling the SM is determined by the vacancy formation energy and the migration energy as shown in Eq. (13). It is plausible to expect that the values of these energies depend upon the cluster size like other physical properties exhibiting the size effect. In fact, there are several theoretical studies which point out that the vacancy formation energy E_f in metal clusters depends on the size in the metal clusters [35–37]. But it has not been well studied how the size effect manifests itself in AH clusters. In order to compute the value E_m , it is necessary to enumerate the reaction paths along which the vacancy hops. Since there also exists a large variety of the saddle points which may contribute to the numerical estimation for E_m , it is practically hard to calculate E_m . Rather than pursuing the role of E_m , in this paper we concentrate on the numerical estimation of E_f . Here we would like to extract an insight about the effect of size upon the enhancement of diffusion by focusing on the size-dependent feature of E_f .

According to the definition of the vacancy formation energy, E_f is the energy which is spent for the process such that a single constituent atom is removed from the target system to the surface. Let us apply that definition to calculate E_f of clusters which have the same number of atoms but different cluster shapes. The value E_f would depend on the shapes even if the number of the constituent atoms is the same, because the energy needed to put a single atom on the surface depends upon the detailed structure of the surface. To avoid the difficulty of accounting for the complicated shape-dependence of the cluster, we evaluated E_f of KCl-KBr clusters for a series of the clusters forming a simple cubic structure represented by $(n \times n \times n)$, locating the vacancy at the center of a cluster. In addition, we applied the following convenient relation to evaluate E_f in a cluster composed of N atoms:

$$E_f(N) = E(N-1, v) - \frac{N-1}{N}E(N, 0), \quad (14)$$

where $E(N-1, v)$ and $E(N, 0)$ are the energy of a cluster including $(N-1)$ and N atoms with and without a vacancy, respectively [35, 37].

There are some issues about the applicability of the above formula to a cluster. Strictly speaking, the formation energy of a vacancy, E_f , should be defined as the difference between the energy of a cluster with a vacancy on the most stable surface position and the energy with the vacancy at a position inside the cluster. However, the latter energy depends on the vacancy's position inside the cluster. Thus, the effective vacancy formation energy should be estimated by averaging E_f s over all the lattice points inside the cluster. The validity of this estimation could be verified by comparing it with another vacancy formation energy which is evaluated by MD simulations. We will discuss such quantitative verification of E_f in clusters in a forthcoming paper. In this paper we only present a rough treatment based on Eq. (14).

In Fig. 14 we show the size-dependence of E_f in various kind of AH clusters; KCl-KBr, NaCl-NaBr, RbCl-RbBr and KBr-KI clusters. It is obvious that E_f for all kind of AH clusters decreases remarkably with decreasing size [38]. Thus

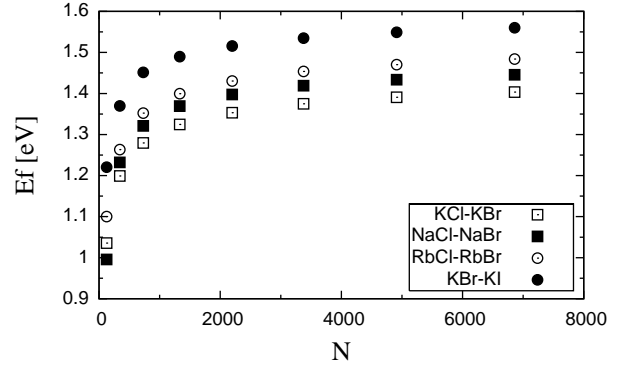


FIG. 14. Size dependence of the vacancy formation energy E_f in KCl-KBr, NaCl-NaBr, RbCl-RbBr and KBr-KI clusters, where N is the number of constituent ions.

the diffusion by vacancies is further enhanced as the size decreases. This is the origin of the size-dependence of activation energy and it is an underlying reason why the Vacancy Mechanism effectively accelerates the SM in a smaller cluster. It is expected that this size-dependence results from the Coulomb long range force interacting between ions in AH clusters. More details for the origin of the size-dependence of vacancy formation energy will be discussed in a forthcoming paper.

VI. CONCLUSION

Rapid diffusion in AH nano clusters, so-called *Spontaneous Mixing*, and its atomistic mechanism were investigated by Molecular Dynamics simulations employing a three dimensional model for ternary alkali halides: KCl-KBr, NaCl-NaBr, RbCl-RbBr and KBr-KI.

To quantify the atomistic mixing process we introduced an indicator, R_g , which is a good indicator of the degree of intermixing in a cubic shape cluster. Applying this indicator to the time evolutions of $(\text{KCl})_{14}(\text{KBr})_{47}$, $(\text{KCl})_{62}(\text{KBr})_{108}$ and $(\text{KCl})_{172}(\text{KBr})_{191}$ and observing their snapshots, we confirmed that the SM is surely reproduced in our model clusters. On the other hand, by computing Lindemann's index, which measures the relative fluctuation of the distance between any two atoms, we proved that the intermixing process proceeds in the solid phase. Similar results were also obtained for AH clusters with different combination of species such as $(\text{NaCl})_{14}(\text{NaBr})_{47}$, $(\text{RbCl})_{14}(\text{RbBr})_{47}$ and $(\text{KBr})_{14}(\text{KI})_{47}$.

The analysis of MD simulations at 600-900 K indicated the Arrhenius type temperature-dependence of the time required for the intermixing. By fitting with Arrhenius law, we also estimated the activation energy: $E_{act} = 0.98, 1.1$ and 1.4 eV for $(\text{KCl})_{14}(\text{KBr})_{47}$, $(\text{KCl})_{62}(\text{KBr})_{108}$ and $(\text{KCl})_{172}(\text{KBr})_{191}$, respectively. It was also confirmed that the activation energy as well as the intermixing time depend on the size of the clusters.

To clarify the atomistic mechanism of the diffusion, we scrutinized surface melting and the dynamics of ions inside the AH clusters during the intermixing. A detailed evalua-

tion of individual Lindemann's index δ_i reveals a very important fact: in contrast to the metal nano clusters the surface melting, which is the necessary condition for Surface Peeling Mechanism, was not observed at all in $(\text{KCl})_{172}(\text{KBr})_{191}$. At the same time, we observed that the time evolutions of radial distance r_i^c of inner ions together with the snapshots of the position of all ions projected onto three planes also do not show any indication of collective motions peculiar to the Surface Peeling Mechanism. All the examples studied in our simulations indicate individual diffusive motions rather than collective motions dominate the mixing process. By visualizing the trajectories of ions we found the Vacancy Mechanism is responsible for the intermixing in AH clusters.

The rough estimation of the diffusion rate D of the intermixing in $(\text{KCl})_{14}(\text{KBr})_{47}$, $(\text{KCl})_{62}(\text{KBr})_{108}$ and $(\text{KCl})_{172}(\text{KBr})_{191}$ at 700 K gave $D = 3.1 \times 10^{-14}$, 1.4×10^{-14} , and 8.6×10^{-16} m^2/s . These rates are much larger than the

diffusion constant of bulk alkali halide crystals $\sim 4 \times 10^{-19}$ m^2/s . These facts support the conclusion that the intermixing observed in our MDs is rapid diffusion peculiar to nano particles.

Finally, evaluation of vacancy formation energy E_f for AH clusters with different species and sizes showed that E_f definitely decreases as the size of the clusters becomes small, which is consistent with the size dependence of activation energy. This decrease of vacancy formation energy with size is the principal origin of the rapidness of SM in AH clusters.

ACKNOWLEDGMENTS

The authors thank M. Ohnishi and M. Watanabe for their preliminary calculation in the early stage of the research. This work is partly supported by JSPS KAKENHI (Grant No.23540459 and 08J08311).

-
- [1] E. L. Wolf, *Nanophysics and nanotechnology* (Wiley-Vch, 2008).
 - [2] G. A. Ozin, A. C. Arsenault, and L. Cademartiri, *Nanochemistry: a chemical approach to nanomaterials* (Royal Society of Chemistry, 2009).
 - [3] M. Haruta, T. Kobayashi, H. Sano, and N. Yamada, *Chem. Lett.* **16**, 405 (1987).
 - [4] M. Haruta, *Nature* **437**, 1098 (2005).
 - [5] H. Yasuda and H. Mori, *Z. Phys. D* **31**, 131 (1994).
 - [6] H. Yasuda, H. Mori, M. Komatsu, K. Takeda, and H. Fujita, *J. Electron Microsc.* **41**, 267 (1992).
 - [7] H. Yasuda and H. Mori, *Phys. Rev. Lett.* **69**, 3747 (1992).
 - [8] Y. Kimura, Y. Saito, T. Nakada, and C. Kaito, *Phys. Low-Dim. Struct.* **1/2**, 1 (2000).
 - [9] Y. Kimura, Y. Saito, T. Nakada, and C. Kaito, *Physica E* **13**, 11 (2002).
 - [10] Y. Shimizu, S. Sawada, and K. S. Ikeda, *Eur. Phys. J. D* **4**, 365 (1998).
 - [11] Y. Shimizu, K. S. Ikeda, and S.-i. Sawada, *Phys. Rev. B* **64**, 075412 (2001).
 - [12] R. Garrigos, P. Cheyssac, and R. Kofman, *Z. Phys. D* **12**, 497 (1989).
 - [13] K. F. Peters, J. B. Cohen, and Y.-W. Chung, *Phys. Rev. B* **57**, 13430 (1998).
 - [14] T. R. Kobayashi, K. S. Ikeda, Y. Shimizu, and S. Sawada, *Phys. Rev. B* **66**, 245412 (2002).
 - [15] T. R. Kobayashi, K. S. Ikeda, Y. Shimizu, and S. Sawada, *J. Chem. Phys.* **118**, 6552 (2003).
 - [16] S.-i. Sawada, Y. Shimizu, and K. S. Ikeda, *Phys. Rev. B* **67**, 024204 (2003).
 - [17] F. Baletto, C. Mottet, and R. Ferrando, *Phys. Rev. Lett.* **90**, 135504 (2003).
 - [18] M. Born and J. E. Mayer, *Z. Phys. A* **75**, 1 (1932).
 - [19] F. G. Fumi and M. P. Tosi, *J. Phys. Chem. Solids* **25**, 31 (1964).
 - [20] M. P. Tosi and F. G. Fumi, *J. Phys. Chem. Solids* **25**, 45 (1964).
 - [21] A. Aguado, *J. Phys. Chem. B* **105**, 2761 (2001).
 - [22] J. Jellinek, T. L. Beck, and R. S. Berry, *J. Chem. Phys.* **84**, 2783 (1986).
 - [23] M. P. Allen and D. J. Tildesley, *Computer Simulation of Liquids* (Oxford University Press, 1989).
 - [24] T. Niiyama, Y. Shimizu, T. R. Kobayashi, T. Okushima, and K. S. Ikeda, *Phys. Rev. E* **79**, 051101 (2009).
 - [25] Note that $(\text{KCl})_{14}(\text{KBr})_{47}$ rarely causes large-scale structural transition from a simple cubic shape to a rectangular parallelepiped by shear deformation along a diagonal line on a surface. But such events are so rare that we ignored several MD runs including these events (in fact, we cannot observe the events in larger clusters, $(\text{KCl})_{62}(\text{KBr})_{108}$ and $(\text{KCl})_{172}(\text{KBr})_{191}$).
 - [26] S. Sugano, Y. Nishina, and S. Ohnishi, *Microclusters* (Springer, 1987).
 - [27] P. G. Shewmon, *Diffusion in Solids* (McGraw-Hill, Inc., New York, 1963).
 - [28] C. Kittel, *Introduction to solid state physics*, 8th ed. (Wiley, 2005).
 - [29] R. Kofman, P. Cheyssac, R. Garrigos, Y. Lereah, and G. Deutscher, *Physica A* **157**, 630 (1989).
 - [30] T. Zykova-Timan, D. Ceresoli, U. Tartaglino, and E. Tosatti, *Phys. Rev. Lett.* **94**, 176105 (2005).
 - [31] S. Pehkonen, M. Ahtee, and O. Inkinen, *J. Phys. D* **5**, 767 (1972).
 - [32] S. Pehkonen, *J. Phys. D* **6**, 538 (1973).
 - [33] N. Laurance, *Phys. Rev.* **120**, 57 (1960).
 - [34] H. Mizuno and M. Inoue, *Phys. Rev.* **120**, 1226 (1960).
 - [35] M. Sinder, D. Fuks, and J. Pelleg, *Phys. Rev. B* **50**, 2775 (1994).
 - [36] W. H. Qi and M. P. Wang, *Physica B* **334**, 432 (2003).
 - [37] M. Müller and K. Albe, *Acta Mater.* **55**, 3237 (2007).
 - [38] T. Niiyama, S.-i. Sawada, K. S. Ikeda, and Y. Shimizu, *Chem. Phys. Lett.* **503**, 252 (2011).